

PROCEEDINGS OF SPIE

[SPIDigitalLibrary.org/conference-proceedings-of-spie](https://spiedigitallibrary.org/conference-proceedings-of-spie)

A comparative study of charge transfer inefficiency value and trap parameter determination techniques making use of an irradiated ESA-Euclid prototype CCD

Thibaut Prod'homme, P. Verhoeve, R. Kohley, A. Short, N. Boudin

Thibaut Prod'homme, P. Verhoeve, R. Kohley, A. Short, N. Boudin, "A comparative study of charge transfer inefficiency value and trap parameter determination techniques making use of an irradiated ESA-Euclid prototype CCD," Proc. SPIE 9154, High Energy, Optical, and Infrared Detectors for Astronomy VI, 915409 (23 July 2014); doi: 10.1117/12.2054862

SPIE.

Event: SPIE Astronomical Telescopes + Instrumentation, 2014, Montréal, Quebec, Canada

A comparative study of charge transfer inefficiency value and trap parameter determination techniques making use of an irradiated ESA-Euclid prototype CCD

T. Prod'homme^{*a}, P. Verhoeve^a, R. Kohley^b, A. Short^a, N. Boudin^a

^aEuropean Space Agency, ESTEC, Keplerlaan 1, 2200AG Noordwijk, The Netherlands;

^bEuropean Space Agency, ESAC, P.O. Box 78, E-28691 Villanueva de la Cañada, Madrid, Spain

ABSTRACT

The science objectives of space missions using CCDs to carry out accurate astronomical measurements are put at risk by the radiation-induced increase in charge transfer inefficiency (CTI) that results from trapping sites in the CCD silicon lattice. A variety of techniques are used to obtain CTI values and derive trap parameters, however they often differ in results. To identify and understand these differences, we take advantage of an on-going comprehensive characterisation of an irradiated Euclid prototype CCD including the following techniques: X-ray, trap pumping, flat field extended pixel edge response and first pixel response. We proceed to a comparative analysis of the obtained results.

Keywords: CCD, Radiation damage, CTI, Bulk traps, Euclid, X-ray, Trap-pumping, FPR, EPER

1. INTRODUCTION

Radiation-induced charge transfer inefficiency (CTI) is now a well-identified threat to the science objectives of space missions making an extensive use of CCDs to acquire with great accuracy astrometric, photometric, spectroscopic, or morphologic measurements of distant light sources. Defects (also referred to as traps) in the silicon lattice of the CCD stochastically capture and release the signal carriers during their transfer decreasing the CTI and creating characteristic spurious trails after each source. The image distortion and the decrease in signal-to-noise ratio introduce measurement biases as well as an irreversible loss of best-achievable accuracy [1, 2, 3, 4].

In the past years a wealth of studies has shed light on this particular issue, especially in the context of the Hubble Space Telescope image processing [e.g., 5, 6] and the preparation of the ESA missions: Gaia [1, 2] and Euclid [3,4]. These studies have stressed the importance of characterizing the CCD CTI performance and trap properties pre and post irradiation as a function of the temperature, clocking scheme, and transfer rate. This detailed characterisation with the support of modelling is key to design a proper CTI mitigation scheme that often consists in a set of hardware and software CTI countermeasures; most commonly the optimization of the CCD operating conditions accompanied by algorithms in the on-ground data processing and in-orbit calibration means.

While CTI values are often used as a requirement in the design and acceptance of CCDs for space missions, the trap parameters are used as input in recent CTI-mitigation algorithms using forward modelling of the charge transfer and trapping. Used in on-ground characterization campaigns or during operation for calibration purposes, a variety of techniques are available to determine both CTI values and trap properties; they however often provide us with different results.

In an effort to achieve a better understanding of these differences and to compare the nature of the identified traps for each technique we take advantage of the comprehensive characterisation of an irradiated Euclid CCD prototype – taking place at ESA/ESTEC – to support the Euclid Consortium in designing and testing a dedicated CTI mitigation scheme. This characterisation involves basic CCD characteristics determination (e.g. quantum efficiency, readout noise) [7], the projection of a realistic Euclid-like scene to directly assess the impact of CTI on the Euclid galaxy shape measurement [8], and a CTI value and trap parameter determination exercise using common techniques: X-ray, Extended Pixel Edge (EPER) and First Pixel Response (FPR), and trap pumping. After giving a brief summary of each of these techniques, we compare and discuss the results obtained for parallel and serial CTI values, image area and serial register trap species density, as a function of temperature, signal level, clocking scheme, and radiation dose.

*thibaut.prodhomme@esa.int

2. TESTED DEVICE CHARACTERISTICS, OPERATION, AND IRRADIATION

The tested device is an e2v CCD 273 with serial number 11263-07-01 manufactured as part of the Euclid CCD pre-development phase. Specially designed by e2v for the Euclid mission, it is a back illuminated red-enhanced 40 μm -thick device comprising an array of 4kx4k light-sensitive pixels, 4 output nodes, and a charge injection structure along the horizontal direction located at the center of the device. Its main characteristics are summarized in Table 1, and the CTI requirements are detailed in Table 2 (see [9] for a complete description). Note that to improve serial CTI at lower signal levels the width of the register channel has been reduced.

Table 1. Summary of the main specifications of the e2v CCD 273.

Parameter	Specification	Comments
Image format	4132×4096 parallel×serial pixels	~5x5 cm^2 sensitive area
Pixel size	12x12 μm^2	
Number of phases	image area: 4, serial register: 3	
Operating mode	Back-illuminated, non-inverted	Back-thinned to 40 μm
Amplifier responsivity	6-8 $\mu\text{V}/\text{electron}$	4 amplifiers
Read noise	<3.6 electron rms	@ 70 kHz pixel rate
Full Well Capacity	> 175 k electrons	
Dark signal	<6×10 ⁻⁴ electrons/pixel/s	@ T=153K
Quantum efficiency	>83%, >83%, >23%	@ 550, 750 and 950nm

Table 2. Charge Transfer Inefficiency (CTI) requirements on the Euclid CCD at beginning of life (native) and following irradiation with a 10MeV equivalent non-ionizing radiation dose of 5x10⁹ protons.cm⁻² [9]

Direction	Native CTI	CTI post irradiation	Comments
Parallel	5.0 10 ⁻⁶	5.5 10 ⁻⁵	Measured using X-ray Fe55
Serial	5.0 10 ⁻⁶	4.0 10 ⁻⁵	Measured using X-ray Fe55

The CCD was irradiated at Kernfysisch Versneller Instituut (Groningen, The Netherlands) in April 2013. The irradiation was performed at room temperature using a 38.5 MeV primary proton beam degraded to 10.4 MeV. Using two different shielding masks (see Fig. 1) and irradiation durations, half the bottom left quadrant (readout node F) received a 2.4 10⁹ protons cm⁻² (10 MeV equivalent) fluence and the top right and left quadrant halves (H and G) received a 4.8 10⁹ protons cm⁻² fluence – the Euclid requirement level for end-of-life (eol) solar proton fluence. These two irradiation levels are later referred to as eol/2 and eol. The charge injection structure, the entire E quadrant, the serial register of the H quadrant, and the four output nodes were not irradiated. Following the irradiation the CCD was stored at room temperature and repeatedly cooled down to 153 K for measurement. Fig. 1 (right) shows a dark frame acquired after irradiation at warm temperature and gives an overview of the irradiation pattern.

During characterisation, the CCD was operated in nominal Euclid conditions i.e. at a readout frequency of 70 kHz, and a temperature of 153 K unless mentioned otherwise. The exact Euclid CCD clocking scheme is still to be determined; several optimizations to reduce CTI are currently under investigation [10, 11]. We make use of an even serial clocking scheme (i.e. same clock width for each register phase at each step) that minimizes serial CTI but a non-optimized nominal line/parallel transfer duration of 0.11 ms. In Section 4 we investigate the effect of longer line transfer durations on parallel CTI.

We used the ESA Payload Technology Validation section CCD test bench located at ESTEC (Noordwijk, The Netherlands). A comprehensive description of the data acquisition system, driving electronics, temperature and vacuum control system can be found in [7].

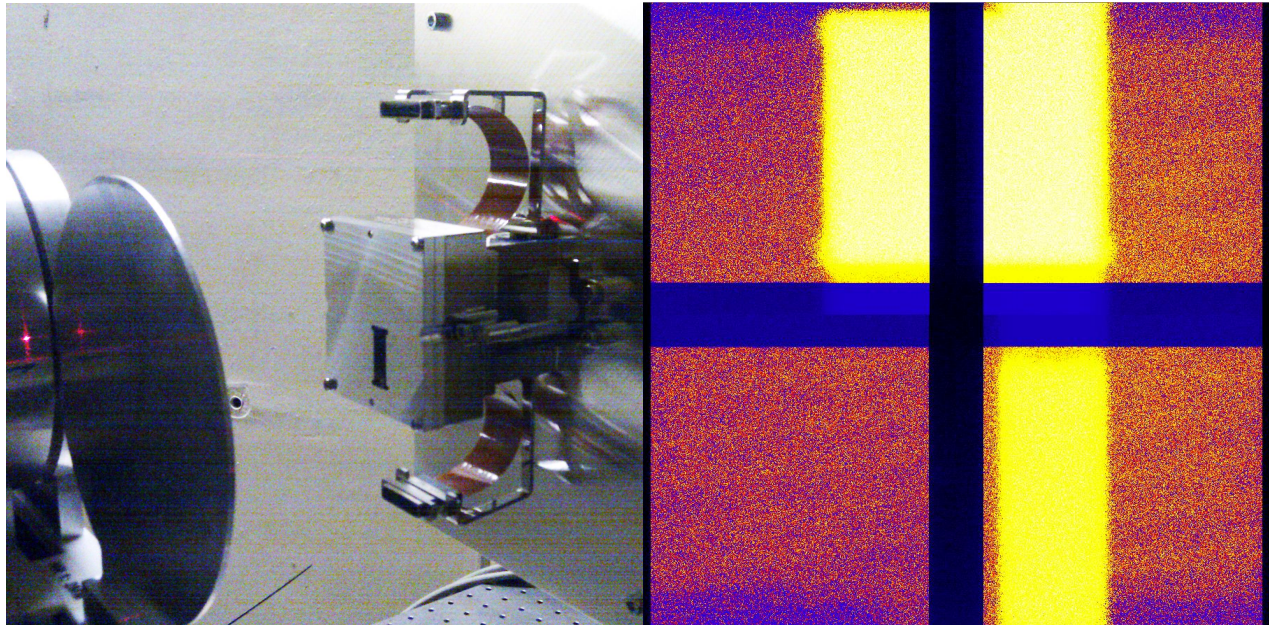


Figure 1. Left: Photograph taken during the beam alignment procedure prior to irradiation with the Euclid CCD and its Aluminum shield mounted. Right: Dark frame taken post irradiation (1,000 s at 214 K) showing the irradiated zones (in bright yellow). The central dark blue regions are the parallel and serial over-scans. As expected the bottom right irradiated region ($2.4 \cdot 10^9$ protons cm^{-2}) shows less dark current than the top irradiated regions ($4.8 \cdot 10^9$ protons cm^{-2}).

3. CTI AND TRAP CHARACTERISATION TECHNIQUES

This section gives the necessary background to each of the techniques we used, for the understanding and interpretation of the results in Sections 4 and 5. More detailed descriptions can be found in [12]. We recall that CTI corresponds to the fraction of charge lost at each pixel transfer. E.g. for a parallel CTI value of $5 \cdot 10^{-6}$, 0.0005% of the charge packet is lost at each transfer in the parallel direction (line transfer), and 1% of the charge packet is lost after 2,000 transfers. The trap density (the average number of traps per pixel) can be estimated from the CTI value (and vice versa) assuming a trap can capture a single electron at a time:

$$\rho = \text{CTI} \times \text{signal level} = \text{total charge loss} / \text{number of transfers}$$

3.1 X-ray

CTI (as well as gain and readout noise) can be determined by using 5.9 keV X-ray photons from a ^{55}Fe source. Each X-ray photon generates about 1,600 e^- (at $T = 153$ K), however due to CTI the number of electrons reaching the output node decreases as a function of the number of transfers; this is illustrated in Fig. 2. We determine CTI by selecting all the single-pixel X-ray events in a region of interest (irradiated or reference region) and performing a linear fit to these event values as a function of the number of transfers in either the parallel or the serial direction. A similar fit is made to the pixel values of the ‘empty’ pixels in order to determine any slope in the offset (e.g. due to dark current generated during readout). The CTI is then found as the slope of the fit to the single pixel event pixel values, corrected for any slope in the offset.

X-ray data was acquired at 5 different temperatures in the range 143-183 K, using an X-ray density of ~ 80 pixels/photon (controlled with exposure time). Note that the greater the number of X-ray events is, the smaller the measured CTI value will be. This is because traps with release time constants longer than the transfer duration remain filled after the capture of the first X-ray event electrons to be transferred and cannot capture when the following events are transferred. A series of X-ray frames was also acquired for different line transfer durations at $T = 153$ K.

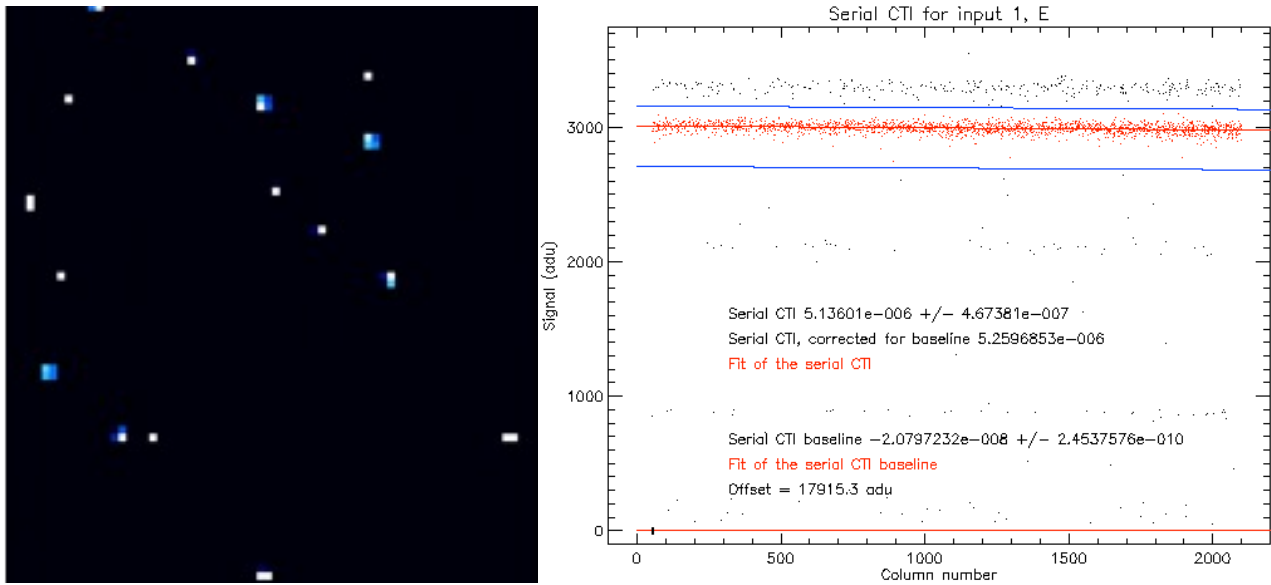


Figure 2. Left: A typical image containing single-pixel and split X-ray events. Right: Single-pixel X-ray event signal values (black and red dots) are plotted against the number of serial transfers. A slight but visible slope shows the decrease in X-ray event signal values with the number of transfers, serial CTI is determined by measuring this slope, using Mn-K α events (red dots) only.

3.2 Trap pumping

Trap pumping – more commonly called pocket pumping – consists in exposing the CCD to a flat field (a uniform level of illumination) and clocking the CCD backward and forward for a number of cycles, effectively transferring multiple times the charge packets back and forth over the same location on the CCD. When this process occurs next to a trap site, a high-low or low-high signal level dipole may appear in the image (cf. Fig. 3, left): depending on the exact trap location and the trap capture and release rates, charge can be successively moved (or pumped) from one charge packet to the next, resulting in a depleted charge packet adjacent to a charge packet with an increase number of electrons. By counting the number of dipoles in one image one can get a rough estimate of the trap density and henceforth measure a CTI value.

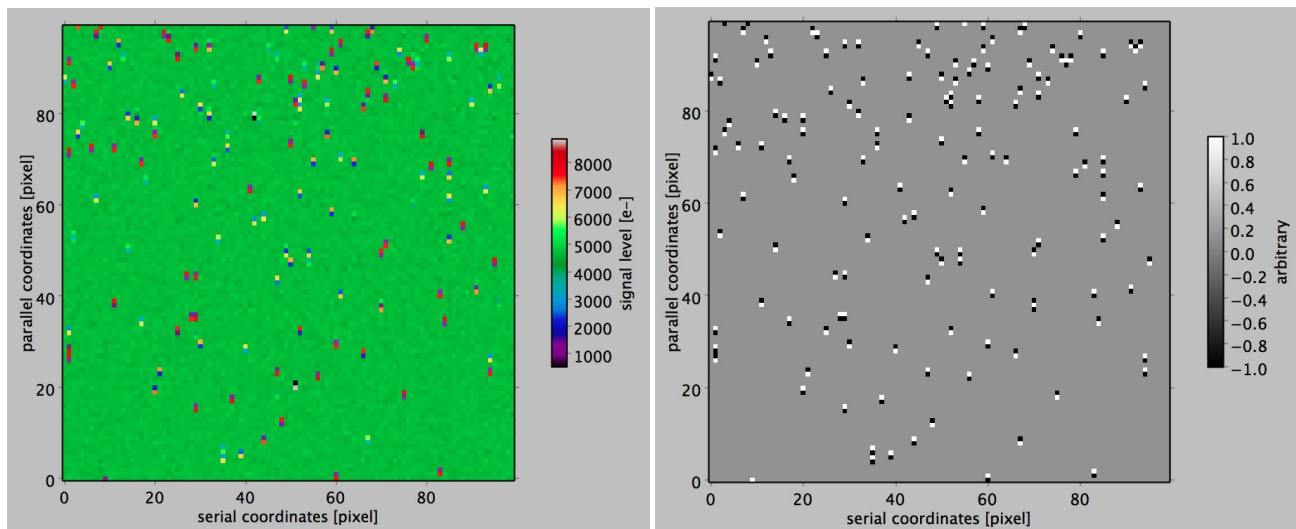


Figure 3. Left: Close-up on a trap-pumping image obtained for a flat field level of about 4,500 e $^-$ and 4,000 parallel pumping cycles. Dipoles of different colours show the trap locations for traps with different trapping efficiencies. Right: For the same image, the detected dipoles after applying our dipole detection algorithm using a trapping efficiency threshold of 20%.

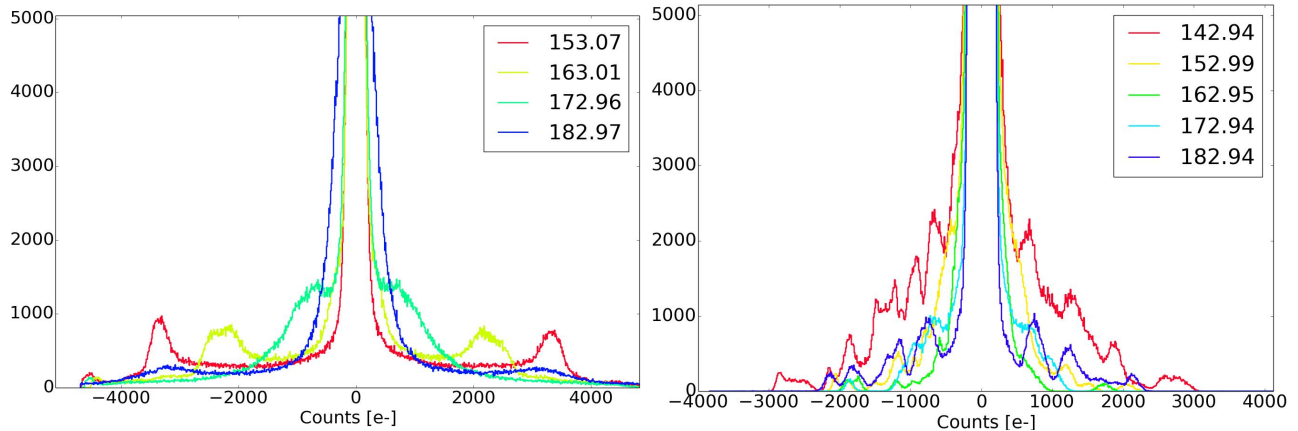


Figure 4. Image pixel value histograms obtained over the CCD irradiated regions (eol) for parallel (left) and serial (right) pumped frames at different temperatures. The histograms are centered on 0 because the median image value (roughly corresponding to the flat field level) is subtracted from the image before analysis. The flat field level was about 4,000 e⁻ and the number of cycles 4,000. The peak at higher values as a counter part at lower values, characteristic of the observed dipoles (Fig. 3). The trap capture efficiency determines the position of the peaks. Traps in the image area (left) show a single efficiency peak at each temperature, while serial register traps show a number of peaks varying in location and intensity with the temperature.

To count dipoles one needs to delimit intervals for high and low dipole values; these intervals can be defined in terms of trapping efficiency threshold. If a charge is pumped every two cycles (effectively moved from one packet to the next), the trapping efficiency is 50%. Assuming a particular flat field level S_{ff} and a number of pumping cycles N , if one applies an efficiency threshold of 20% in the selection of dipoles, pixel values S_{pix} in the interval $[S_{ff} - 0.2 \times N, S_{ff} + 0.2 \times N]$ are discarded from the analysis.

Fig. 4 shows image pixel value histograms for the CCD irradiated regions at different temperatures. Fig. 4 left shows the image histogram obtained when the CCD is clocked backward and forward 4,000 times in the parallel direction and Fig. 4 right in the serial direction. For $T = 153$ K and parallel pumping (Fig. 4, left, red line), a single peak is present at high signal level close to 4,000 e⁻ (after the median image level is removed) showing a single population of trap in terms of efficiency close to 100%. The left histograms show that when the temperature increases, the trapping efficiency decreases until the dipole peaks disappear in the central flat field peak.

A great deal of information can be inferred from trap pumping data (e.g. [13]), however one should note that the analysis is complicated by the number of clock phases. In this study we focus exclusively on the trap (or dipole) density. Data was obtained for a flat field level of about 4,500 e⁻ and 4,000 pumping cycles at different temperatures in the interval [143-183] K. Parallel pumping data was also obtained for different line transfer durations.

3.3 Flat field EPER and FPR

FPR consists in studying the charge loss occurring as a result of CTI in the front edge of block of charges transferred throughout the CCD in either the parallel or serial directions (see Fig. 5 right), while EPER focuses on the charge release after a similar charge block. A block – a set of consecutive lines or rows at the same signal level – can be generated using different techniques such as charge injection, clock-induced charge injection, or a uniform level of illumination combined with a specific readout configuration and clocking scheme.

The Euclid device comprises 4 output nodes and thus offers a number of readout configurations. The CCD can be read out using all four output nodes effectively dividing the image into four quadrants, or using two output nodes only splitting the image in two halves (top and bottom).

To study serial EPER, we illuminate the CCD with a flat field, read it out using the four output nodes, and operate more serial transfers than the number of light sensitive pixels in the serial direction to obtain a serial overscan region free of illumination and containing the released charge.

Studying serial FPR requires two types of frames: a ‘reference’ frame and a ‘FPR’ frame. To obtain the reference frame we illuminate the CCD with a flat field and use a two-output node readout. To obtain the FPR frame, we proceed in the same way but at each line readout the first (serial) half of the image is dumped. We then compute the charge loss by subtracting the FPR median serial profile to the reference median serial profile.

Lastly to study the parallel FPR and EPER, we illuminate the CCD and clock the CCD backward in the parallel direction for a certain number of transfers. At each line transfer, the furthest line (from the serial register) is dumped in the charge injection structure in the middle of the device. In this way we can create a block of charge of any parallel width starting from the charge injection structure. Once the charge block is created we can read out the CCD using the four output nodes. We use the parallel overscan to study the charge release occurring after the block. To compute the charge loss in the block leading edge, we subtract the median parallel profile in the irradiated region to the reference median parallel profile (obtained in the CCD non-irradiated region). EPER and FPR data was obtained at different temperatures, for different flat field levels (controlled with exposure time), and two line transfer durations.

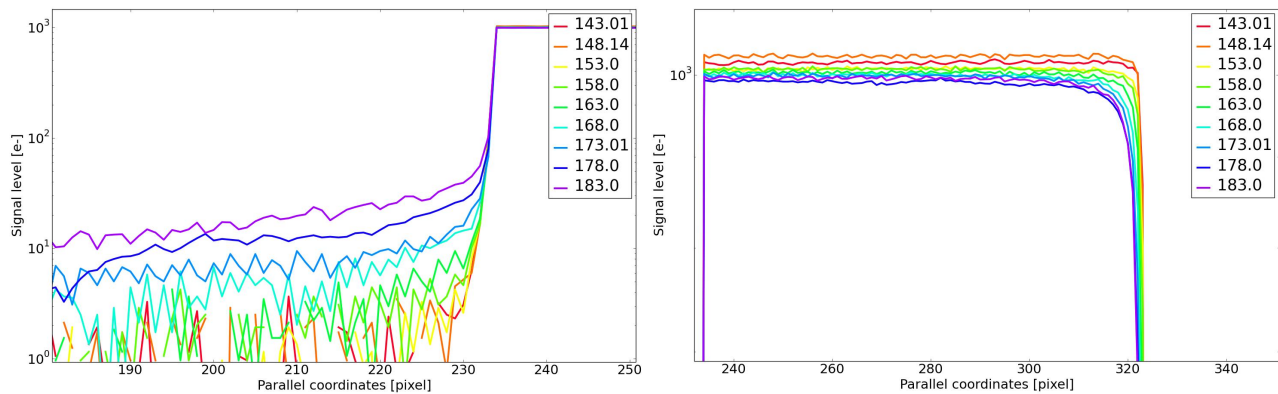


Figure 5. Example of parallel median profiles after a block of charge (left) and at the front edge of the same block (right) for different temperatures (signal level scale is logarithmic). EPER is extracted from summing up electrons in the charge release trail (left), while FPR is measured from the charge loss occurring in the first pixel of the charge block (right). Note that the transfer direction is left-to-right in both panels.

4. CTI MEASUREMENT AND TRAP DENSITY COMPARISON

In this section we present and compare the results obtained for each technique as a function of temperature, line transfer duration, and signal level. Each time we detail the measured CTI and trap density values for the different irradiation levels.

4.1 As a function of temperature

Figure 6 shows a comparison between parallel CTI values and image area trap densities in the CCD measured using X-ray, trap pumping, and flat-field FPR/EPER in the irradiated (eol in red, eol/2 in orange) and reference (blue) regions as a function of temperature in the range [143-183] K. We recall that the nominal temperature of operation for the Euclid CCD is 153 K. Figure 7 shows similar results obtained for serial CTI and trap density in the serial register.

To convert from CTI to trap density and vice versa we need to estimate the signal level at which the technique was applied. For X-ray, the single-pixel X-ray events from which the charge loss is measured contain about $1,600 e^-$ (at $T = 153$ K). For trap pumping, the signal level considered is the level of flat field illumination (about $4,500 e^-$) that is measured for each image at each temperature. For the flat-field FPR and EPER technique, the determination of a reference signal level to compute a CTI value from the derived trap density is less straightforward. The charge loss and charge release are measured over a certain number of pixels (in our case 12) in the charge block leading edge or in the charge release trail following the same charge block. It is not clear which level should be chosen: the flat field level, or the total number of charges in the preceding block for EPER, or the flat field level times the number of leading-edge pixels considered in the charge loss measurement for FPR. For parallel CTI, to avoid ambiguities we compute the CTI

· Note that we ignored the temperature variation of the silicon bandgap that affects the number of electrons generated by the 5.9 keV X-ray photons, and used the $1.6 ke^-$ value at all temperatures.

values only using FPR measured in the first pixel of the block leading edge. Hence the flat field level can be used, in this case $1,000 e^-$. FPR measurement as a function of temperature being not available in the serial direction, we use the EPER measurement (over 12 pixels) and the flat field level of illumination $1,000 e^-$.

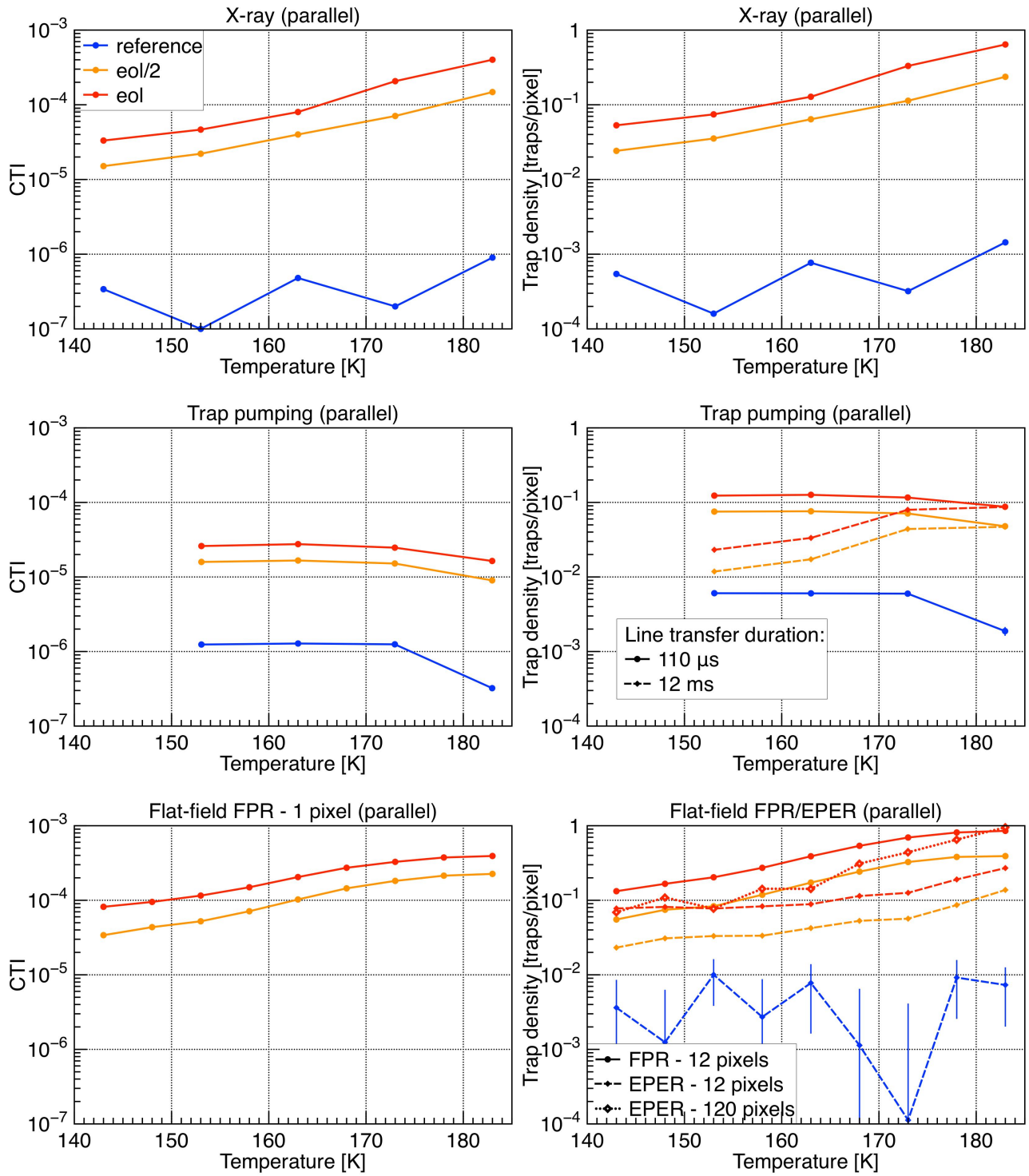


Figure 6. Parallel CTI values (left) and image area trap densities (right) as a function of the temperature as measured by X-ray (top), trap pumping (middle), and flat-field FPR/EPER (bottom).

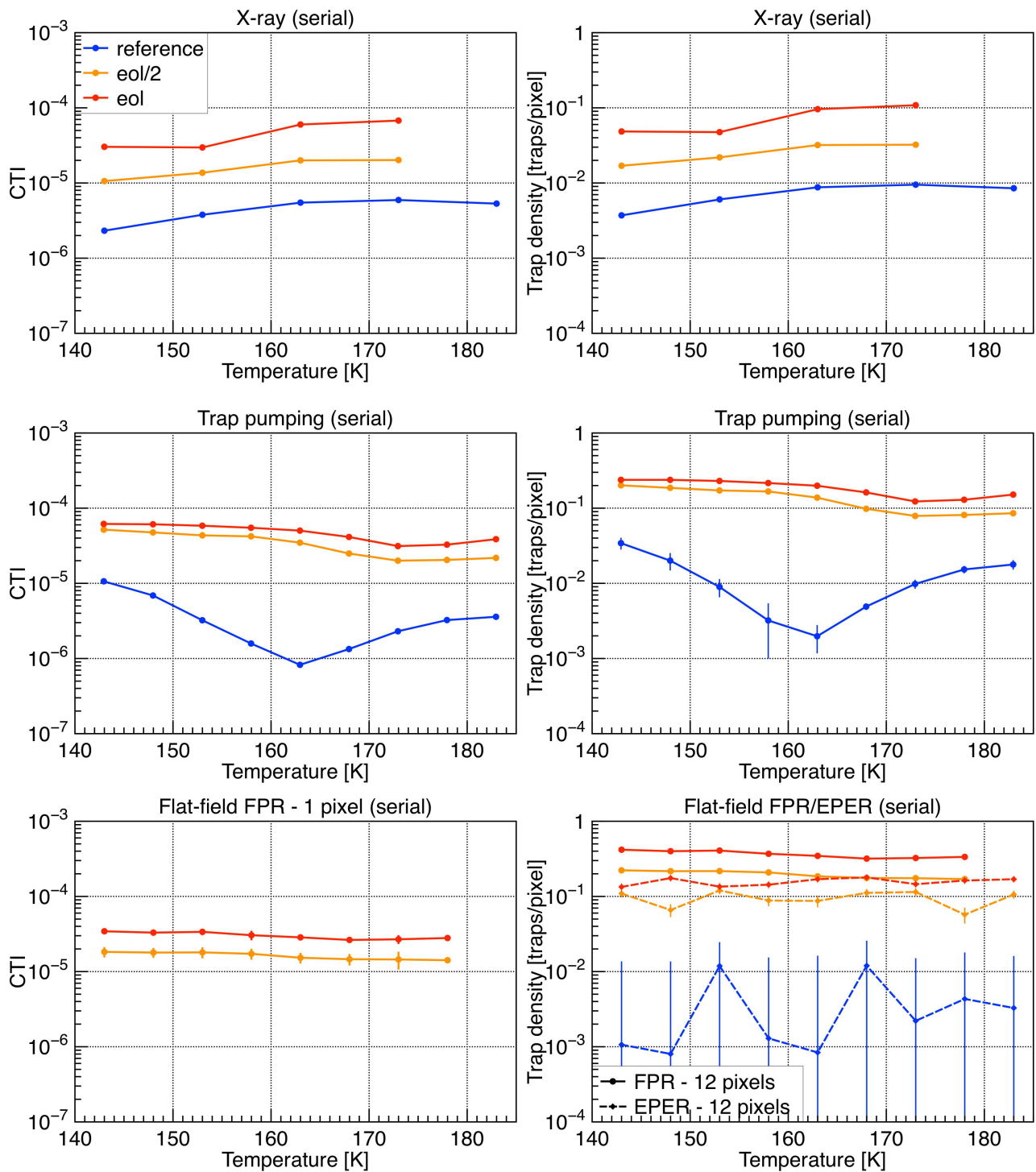


Figure 7. Serial CTI values (left) and serial register trap densities (right) as a function of the temperature as measured by X-ray (top), trap pumping (middle), and flat-field FPR/EPER (bottom).

Fig. 6 (left, blue lines) shows that reference (or native) parallel CTI values (i.e. obtained over non-irradiated CCD regions) range from 10^{-7} to $2 \cdot 10^{-6}$ better than the requirement level ($5 \cdot 10^{-6}$ at $T = 153$ K, see Table 2) indicating good native CTI performance. The temperature trends differ for X-ray and trap pumping (reference parallel CTI cannot be measured using FPR cf. the previous section).

Fig. 7 (left, blue lines) indicates a native serial CTI (Fig. 7) ranging between 10^{-7} and 10^{-5} and a significant variation depending on the measurement technique. Nevertheless at $T = 153$ K we measure for all techniques a CTI value below the requirement level of $5 \cdot 10^{-6}$. Temperature trends vary again with the measurement technique.

Comparing the red (eol) and orange (eol/2) lines in Fig. 6 and 7, one notes that as expected CTI values generally scales linearly with the radiation dose (except for the serial trap pumping results). Parallel radiation-induced CTI values are greater by at least an order of magnitude than native CTI values. The increase in serial CTI due to radiation damage is of at worst one order of magnitude, and thus less dramatic than for parallel CTI but for poorer native performance. Both post-irradiation serial and parallel CTI requirements at $T = 153$ K are generally met.

Parallel CTI (and trap density) increases with the temperature for the X-ray and FPR/EPER measurement, but is rather flat and tends to decrease for trap pumping. One potential explanation is that different techniques probe different trap species. EPER is measured in the first 12 pixels of the release trail and hence probes traps with rather short release time constant (compared to the parallel transfer time), FPR is sensitive to the capture and thus to 'all' traps. Fig. 6 bottom right shows the trap density as a function of temperature for both FPR and EPER (i.e. all traps vs. shorter release time constant traps). We note that the trap-pumping trend is not reproduced by neither FPR nor EPER. Fig. 6 middle right panel shows the effect of increasing the line transfer duration (dashed line), i.e. losing sensitivity to shorter release time constant traps. We now observe an apparent decrease of trap density with decreasing temperature, recovering a similar trend as for X-ray and FPR/EPER. Again for serial CTI and trap density in the serial register the temperature trends for each technique are different complicating further the optimization process.

Now when comparing trap density values for each technique, we note that for both image area and serial register traps the measured native density is generally lower than 0.01 traps pixel^{-1} . After irradiation, the measured image area trap density can increase up to close to 1 trap pixel^{-1} for the highest temperature (X-ray and FPR/EPER measurements). The serial register trap density remains at a stable level close to 0.1 traps pixel^{-1} , similar to the parallel trap density at lower temperatures.

In the parallel case (Fig. 6) trap pumping seems to underestimate the trap density when compared to FPR/EPER and X-ray results especially at higher temperatures; although one expects a greater trap density measured by trap pumping due to a higher probing signal level (4,500 e- compared to 1,600 and 1,000 e- for respectively the X-ray and FPR/EPER measurements), we generally notice a similar or smaller measured density. This may be partly imputed to our dipole detection algorithm that was set with a too high trapping efficiency threshold (cf. previous section) missing out the less efficient traps. This is further supported when comparing the difference in measured trap density by the different techniques between the parallel and serial cases: we observe that the difference is less significant for the serial case for which the trapping efficiency threshold was set to a lower value 15% instead of 20%.

Trapping does not vary linearly with the signal level: while the trap density seen by a charge packet increases with the number of charge, the fraction of trapped charge generally decreases with the number of charge. CTI being a measure of the fractional charge loss, it is expected to be smaller for higher reference signal level. For a fairer comparison we should thus repeat this study using a 1,600 e⁻ flat-field level for both FPR/EPER and trap pumping. In the following section, we explore how the trap density varies with signal level.

4.2 As a function of signal level

Figure 8 shows the image area trap densities (left) and the serial register trap densities (right) as a function of the signal level (and for two radiation levels). The figure shows principally the flat field FPR (solid lines) and EPER (dashed lines) measurements. This type of measurement is generally used to derive charge transfer model parameters, in particular related to the relationship between electron density distribution or electron confinement volume and number of electrons (e.g., [14, 15]). In the case of the Euclid CCD the relationship between trap density and signal level is best described by a power law with different components for FPR and EPER, respectively ~ 0.6 and ~ 0.5 .

For a particular radiation level, the FPR measurement of the trap density is always greater than the EPER one. This is expected as the EPER measurement was obtained by summing over only the first 12 pixels of the charge release trail and thus discarding long release time constant traps. Fig. 6 (bottom right panel) shows that considering a greater amount of pixels in the EPER measurement can lead to a greater measured trap density depending on the trap release time constant at play. The difference between FPR and EPER is greater in the parallel case compared to the serial case. This difference increases with signal level.

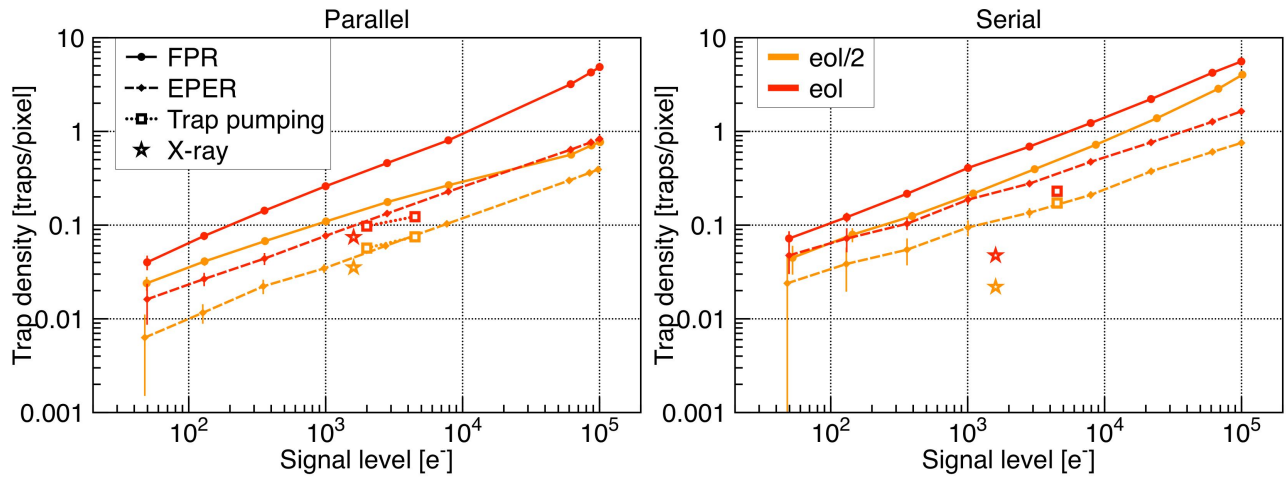


Figure 8. Image area (left) and serial register (right) trap densities as a function of the signal level as measured by FPR (dots), EPER (diamonds), trap pumping (empty squares), and X-ray (empty stars) for two radiation levels (eol: red, eol/2: orange). The trap density roughly follows a power law (both x and y scales are logarithmic). The measurements were performed at a single temperature $T = 153$ K and for a line transfer duration of 0.11 ms.

For comparison Fig. 8 also shows the X-ray measurement at 1,600 e^- (stars) and the trap-pumping measurements (squares) obtained for two different flat field illumination levels: 2,000 and 4,500 e^- . In the parallel case (Fig. 8 left) the trap pumping and X-ray values are in good agreement with the EPER trap density, in particular for the low radiation level. However the serial case (Fig. 8 right) is more problematic with the trap pumping trap density not scaling linearly with the radiation level, and the X-ray measurement underestimating by almost an order of magnitude the trap density (already visible for the lower temperatures in Fig. 7). The latter discrepancy may be explained by the chosen X-ray density; [16] shows that by decreasing the X-ray density one measures a higher trap density in the serial register.

4.3 As a function of line transfer duration

Finally we measure parallel CTI as a function of line transfer duration to study how the three tested techniques compare when used during a clocking scheme optimization exercise. In that case, and as shown in Fig. 9 the same global trend is observed for the three techniques: the longer the line transfer duration is the smaller the CTI. The difference in overall CTI values for each technique varies accordingly to the used probing signal level: CTI is greater for smaller signal levels (1,000 e^- for EPER) than for higher signal levels (4,500 e^- for trap pumping). However the benefit of going to longer line transfer durations varies from a factor 1.3 (X-ray) to 6 (trap pumping) indicating that it is not possible to directly transpose these factors into performance benefit at the instrument level. Similar results and discrepancy were found in [11].

Fig. 10 shows image pixel value histograms for pumped frames with different line transfer durations and illustrates how the trapping efficiency decreases at longer line transfer durations such that the number of detected dipoles decreases.

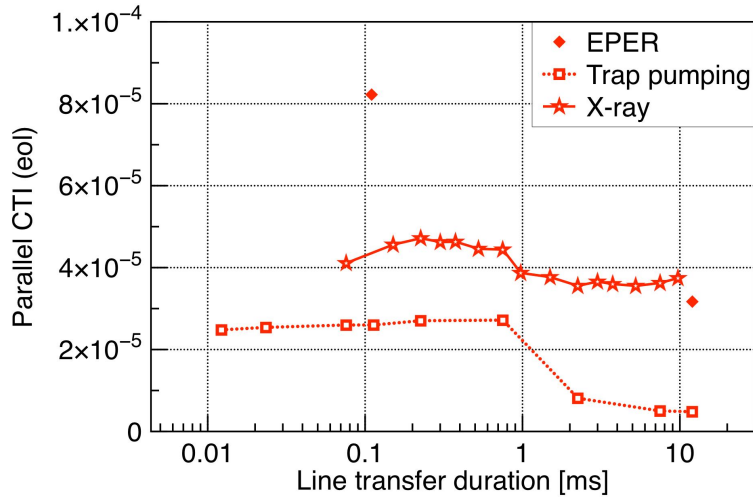


Figure 9. Parallel CTI values as a function of the line transfer duration as measured by X-ray (empty stars), trap pumping (empty squares), and EPER (diamonds). The measurements were performed at $T = 153$ K. Note that the y scale is linear.

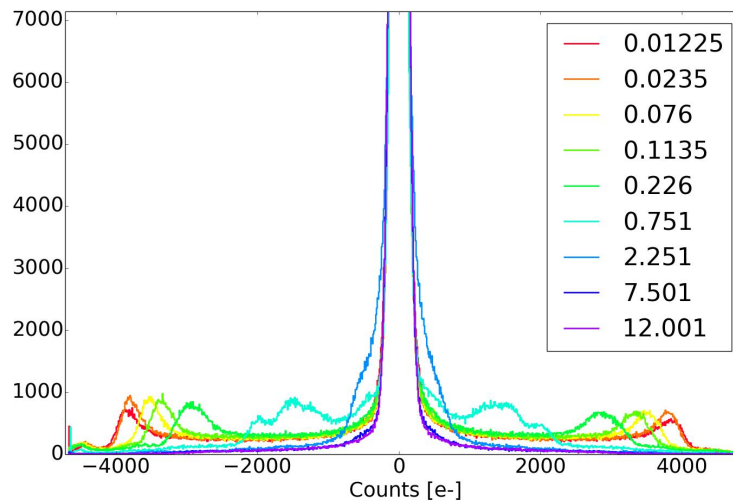


Figure 10. Image pixel value histograms obtained over the CCD irradiated regions (eol) for parallel pumped frames (4,000 cycles, 4,500 e^- flat field level) for different line transfer durations (indicated in ms). To center each histogram on zero, we subtracted the median image value (flat field level). At short line transfer durations the trapping efficiency is close to 100%. The efficiency decreases with the longer line transfer durations until it fades within the flat field peak (located around $0 e^-$). At intermediate line transfer durations (0.75 ms), we note at least two trap populations with different trap efficiencies.

5. CONCLUSIONS

As part of an on-going comprehensive characterisation of an irradiated Euclid CCD prototype, we were able to compare three commonly used CTI value and trap characterization techniques – X-ray, trap pumping, and FPR/EPER – in the context of a temperature and clocking scheme optimization exercise and as a function of signal level. We focused our study on the determination of CTI values and trap densities in the CCD image area and serial register. The tested CCD contained reference (i.e. non-irradiated) regions and irradiated regions representative of the Euclid requirement level for end-of-life solar proton fluence and half of it.

From this comparative analysis, we draw the following conclusions.

CTI values and trap densities measured with each technique are generally within the same order of magnitude, with a better agreement measured for the parallel transfer direction. However the trends with temperature differ significantly from one technique to another, complicating the interpretation of a temperature optimization exercise for instance. Differences between techniques can be attributed to the fact that each technique probes a different slice of the overall trap population. This study gives some insights into which traps are preferentially probed by each technique, but a finer analysis involving the determination of release time constants and capture cross-sections would be required to reach more definite conclusions. Eventually to obtain a fairer comparison, the same study should also be repeated for the exact same probing signal levels.

Increasing the line transfer duration was found beneficial for all techniques, but the improvement factor varies greatly from one technique to another. This indicates that such factors cannot be directly transferred in terms of instrument performance. This poses the question of how representative these techniques are with respect to the nominal CCD operation and the type of measurements carried out during the mission. These techniques are standard tools to obtain reference CTI measurements in the industry and across institutes (X-ray), to calibrate the charge transfer models required for CTI correction in the mission data processing (FPR/EPER), and to obtain the defect locations as well as optimize clocking-schemes against CTI (trap pumping). Yet – as demonstrated by the ambiguity of their results when compared to each other – they cannot replace a more detailed study where the actual mission measurement (astrometry, spectroscopy, shape measurement) is reproduced at least to some extent either in the laboratory or by the mean of modelling.

REFERENCES

- [1] Prod'homme, T. et al., "The impact of CCD radiation damage on Gaia astrometry - I. Image location estimation in the presence of radiation damage," MNRAS, (2012).
- [2] Holl, B. et al., "The impact of CCD radiation damage on Gaia astrometry - II. Effect of image location errors on the astrometric solution," MNRAS, (2012).
- [3] Cropper, M. et al., "Defining a weak lensing experiment in space," MNRAS, (2013).
- [4] Massey, R. et al., "Origins of weak lensing systematics, and requirements on future instrumentation (or knowledge of instrumentation)," MNRAS, (2013).
- [5] Anderson, J. et al., "An Empirical Pixel-Based Correction for Imperfect CTE. I. HST's Advanced Camera for Surveys," PASP, (2010).
- [6] Massey, R. et al. " An improved model of charge transfer inefficiency and correction algorithm for the Hubble Space Telescope," MNRAS, (2014).
- [7] Verhoeve, P. et al., "CCD characterisation for space missions at ESA," Proc. SPIE 9154-15, (2014).
- [8] Prod'homme, T. et al., "Laboratory simulation of Euclid-like sky images to study the impact of CCD radiation damage on weak gravitational lensing," Proc. SPIE 9154-52, (2014).
- [9] Short, A. D. T. et al., "The Euclid VIS CCD detector design, development, and programme status," Proc. SPIE 9154-2, (2014).
- [10] Murray, N.J., et al., "Multi-level parallel clocking of CCDs for: improving charge transfer efficiency, clearing persistence, clocked anti-blooming, and generating low-noise backgrounds for pumping," Proc. SPIE. 8860, (2013).
- [11] Murray, N.J., et al., "Mitigating radiation-induced charge transfer inefficiency in full-frame CCD applications by 'pumping' traps," Proc. SPIE 8453, (2012).
- [12] Janesick, J. et al., [Scientific Charge-Couples Devices], SPIE PRESS, (2011).
- [13] Hall, D. et al., "Determination of In Situ Trap Properties in CCDs Using a "Single-Trap Pumping" Technique," IEEE Transactions on Nuclear Science (2014).
- [14] Short, A. D. T. et al., "An analytical model of radiation-induced Charge Transfer Inefficiency for CCD detectors," MNRAS, (2013).
- [15] Prod'homme, T. et al., "Electrode level Monte Carlo model of radiation damage effects on astronomical CCDs," MNRAS, (2011).
- [16] Verhoeve, P. et al., "Characterisation of CCDs for the EUCLID VIS channel," Proc. Scientific Detector Workshop, (2013).